

# Relativistic Spectra of Hot Black-Hole Winds

Naoko SUMITOMO, Hideki SAITO, and Jun FUKUE

*Astronomical Institute, Osaka Kyoiku University, Asahigaoka, Kashiwara, Osaka 582-8582*

*fukue@cc.osaka-kyoiku.ac.jp*

Kenya WATARAI

*Kanazawa University Senior High School, Heiwamachi, Kanazawa, Ishikawa 921-8105*

(Received 2008 0; accepted 2008 0)

## Abstract

We examine hybrid thermal-nonthermal synchrotron spectra from a spherically symmetric, optically-thin wind, taking into account the relativistic effect. In the relativistic flow from the central object, due to the relativistic beaming effect, the observed spectra often shift towards high frequency and high intensity directions. In the optically thin outflows, however, we find that the intensity of the observed spectra decreases compared with that of the emitted ones, although the peak frequency shifts towards the high frequency direction. This is because in the optically thin outflows we can see the far side flows that go away from the observer. We thus carefully consider optically thin relativistic flows around a black hole such as Sgr A\*.

**Key words:** accretion, accretion disks — black hole physics — Galaxy: center — relativity — winds

## 1. Introduction

It is now well established that black holes with accretion disks and jets are the central engine of various active phenomena, such as active galaxies and quasars, X-ray binaries and micro-quasars, and gamma-ray bursts, and so on (cf. Kato et al. 2008). However, the nature of the central engine is not yet well understood, due partly to poor observational resolutions, and due partly to so many physical complications. In order to clarify the nature of the central engine, many researchers have examined emission spectra and observational appearance of the relativistic flows around black holes. Depending on the mass-accretion and outflow rates, the relativistic flows would be optically thick in some cases while optically thin in other cases.

In any cases, the gravitational energy released in the mass accretion process is converted into the tremendous radiation, magnetic, and kinetic energies. As a result, the relativistic jets and winds often blow off from these systems — a *black hole wind*.

In the optically thick cases, Abramowicz et al. (1991) have pointed out that the optical depth should be carefully considered in the relativistic flows. They found that the shape of the apparent photosphere of a spherical wind becomes concave at a high speed regime due to the relativistic effect on the optical depth.

Recently, furthermore, Sumitomo et al. (2008) has firstly examined the observational appearance of spherically symmetric, relativistic massive winds (see also Fukue & Sumitomo 2009). They also calculated the comoving and observed luminosities, and found that the luminosities increases with the velocity but decreases with the mass-outflow rate.

In the optically thin cases, however, observed spectra of

black-hole winds has not been well examined up to now, in particular the relativistic effect such as Doppler and aberration effects.

In the optically thin relativistic flows, the synchrotron emission is believed to be a key ingredient, and many researchers has discussed its role (Colpi et al. 1984; Begelman & Chiueh 1988; Bisnovatyi-Kogan & Lovelace 1997; Quataert & Gruzinov 1999; Quataert & Narayan 1999; Gruzinov & Quataert 1999; Medvedev 2000). There may exist thermal and non-thermal electrons, and in order to examine the synchrotron emission we should both type of electrons (Zdziarski et al. 1993; Ghisellini et al. 1993; Li et al. 1996; Ghisellini et al. 1998; Özel et al. 2000).

Of these, Özel et al. (2000) obtained the hybrid thermal-nonthermal synchrotron emission spectra from hot accretion flows, and reproduced the observed spectra from the Galactic center source, Sgr A\* (see also Coppi 1999). In their calculations, they considered the hot accretion flow, so called ADAF solutions (Narayan & Yi 1995; Narayan et al. 1996). In addition, they did not considered the relativistic effect in the high velocity regime, where the flow speed is on the order of the speed of light.

Thus, in the present study we consider an optically thin hot wind from a black hole, and examine emitted and observed spectra of hybrid thermal-nonthermal synchrotron emissions, taking into account the relativistic effect in the high velocity regime.

In section 2, the present wind model and the calculation method are briefly described. In section 3 the results are shown. Final section is devoted to concluding remarks.

## 2. Wind Model and Synchrotron Emissivity

In this section we describe the present wind model, and summarize the synchrotron emissivity model.

### 2.1. Wind Model

We assume that a spherically symmetric, relativistic wind blows off from a central object. As a central object, we assume a non-rotating black hole (Schwarzschild black hole); the Schwarzschild radius is defined by  $r_g = 2GM/c^2$ , where  $G$ ,  $M$ , and  $c$  represent the gravitational constant, a black hole mass, and the speed of light, respectively. We use the spherical coordinates  $(R, \theta, \varphi)$  and the cylindrical coordinate  $(r, \varphi, z)$ , whose  $z$ -axis is along the line-of-sight direction.

From continuity equation for the spherically symmetric stationary wind, the rest mass density  $\rho_0$  measured in the comoving frame varies as

$$\rho_0 = \frac{\dot{M}}{4\pi\gamma c\beta R^2}, \quad (1)$$

where  $\dot{M}$  is the mass-outflow rate,  $\beta (= v/c)$  the velocity normalized by the speed of light,  $\gamma = 1/\sqrt{1-\beta^2}$  the bulk Lorentz factor, and  $R = \sqrt{r^2 + z^2}$  a distance from the central object. In the present simple model, the mass-outflow rate  $\dot{M}$  is assumed to be constant, while the wind velocity  $v$  is generally a function of  $R$ .

We further assume that the heating and cooling may be ignored and the wind would expand adiabatically (cf. Park & Ostriker 2007). Then, the temperature  $T_0$  of the wind gas in the comoving frame is proportional to the density as  $T_0 \propto \rho_0^{\Gamma-1}$ , where  $\Gamma$  is the ratio of specific heats and set to be  $5/3$  now. Hence, the comoving temperature varies as

$$\frac{T_0}{T_c} = \left(\frac{R}{R_c}\right)^{-4/3}, \quad (2)$$

where  $T_c$  is the temperature at some reference radius  $R_c$ , that is fixed as  $R_c = r_g$ .

In this paper we assume a one-temperature plasma; i.e., the electron temperature  $T_e$  equals to the ion temperature  $T_0$ . If the flow is not adiabatic but there is energy exchange between ions and electrons, the plasma generally becomes a two-temperature one.

We suppose that the plasma is supplied from the hot gas accretion like ADAF in the equatorial plane including thermal and nonthermal electron populations.

### 2.2. Thermal and Nonthermal Electron Populations

Based upon a model by Özel et al. (2000), we first fix the electron populations with a few parameters. The number density  $N_{\text{th}}$  of electrons in the thermal population is assumed to be sufficiently larger than the number density  $N_{\text{pl}}$  of electrons in the nonthermal population:

$$\frac{N_{\text{pl}}}{N_{\text{th}}} \ll 1, \quad (3)$$

and we set

$$N_{\text{th}} = \rho_0/m_p, \quad (4)$$

where  $m_p$  is the proton mass. That is, it is assumed that the nonthermal electrons do not affect on the flow dynamics and thermal properties, and a large fraction of the electrons in the flow are in a thermal distribution with temperature  $T_e (= T_0)$ .

For the thermal electron population, we use the relativistic Maxwell-Boltzmann distribution:

$$n_{\text{th}}(\gamma_e) = N_{\text{th}} \frac{\gamma_e^2 \beta_e \exp(-\gamma_e/\theta_e)}{\theta_e K_2(1/\theta_e)}, \quad (5)$$

where  $\gamma_e$  is the electron Lorentz factor,  $\beta_e$  is the relativistic electron velocity, and

$$\theta_e = \frac{kT_e}{m_e c^2} \quad (6)$$

is the dimensionless electron temperature, and  $K_2(1/\theta_e)$  is the modified Bessel function of second order. The energy density of this Maxwell-Boltzmann distribution is derived as (Chandrasekhar 1939),

$$u_{\text{th}} = a(\theta_e) N_{\text{th}} m_e c^2 \theta_e, \quad (7)$$

where a coefficient  $a(\theta_e)$  is approximated as (Gammie & Popham 1998)

$$\begin{aligned} a(\theta_e) &\equiv \frac{1}{\theta_e} \left[ \frac{3K_3(1/\theta_e) + K_1(1/\theta_e)}{4K_2(1/\theta_e)} - 1 \right] \\ &\sim \frac{6 + 15\theta_e}{4 + 5\theta_e} \end{aligned} \quad (8)$$

for the present purpose with sufficient accuracy.

For the nonthermal electron population, on the other hand, we use a power-law distribution extending from  $\gamma_e = 1$  to infinity:

$$n_{\text{pl}}(\gamma_e) = N_{\text{pl}}(p-1)\gamma_e^{-p}, \quad (9)$$

where the index  $p$  is a one of free parameters. The energy density of this power-law distribution becomes

$$u_{\text{pl}} = \int_1^\infty \gamma_e m_e c^2 n_{\text{pl}} d\gamma_e = \frac{p-1}{p-2} N_{\text{pl}} m_e c^2, \quad (10)$$

as long as  $p > 2$ .

If we assume that a fraction

$$\eta \equiv \frac{u_{\text{pl}}}{u_{\text{th}}} \quad (11)$$

is constant in any radius, then the number density of the nonthermal electron is related to that of the thermal electron by

$$\frac{N_{\text{pl}}}{N_{\text{th}}} = \eta \frac{p-2}{p-1} a(\theta_e) \theta_e. \quad (12)$$

It should be noted that there is a mistype in equation (8) of Özel et al. (2000).

### 2.3. Synchrotron Emissivity

Next, we summarize the synchrotron emissivity given by Özel et al. (2000) (see also Rybicki & Lightman 1979; Mahadevan et al. 1996).

For the thermal electron population with the relativistic Maxwellian distribution, the synchrotron emissivity  $j_{\nu,\text{th}}$  is approximated as

$$j_{\nu,\text{th}} = \frac{N_{\text{th}} e^2}{\sqrt{3} c K_2(1/\theta_e)} \nu M(x_M). \quad (13)$$

Here,  $\nu$  is the frequency in the comoving frame, and the function  $M(x_M)$  is well approximated by

$$M(x_M) = \frac{4.0505 a}{x_M^{1/6}} \left( 1 + \frac{0.40 b}{x_M^{1/4}} + \frac{0.5316 c}{x_M^{1/2}} \right) \times \exp(-1.8896 x_M^{1/3}), \quad (14)$$

where

$$x_M \equiv \frac{2\nu}{3\nu_b \theta_e^2}, \quad (15)$$

$$\nu_b \equiv \frac{eB}{2\pi m_e c}. \quad (16)$$

The latter  $\nu_b$  is the nonrelativistic cyclotron frequency in a magnetic field of strength  $B$ , which is another free parameter. We set the coefficients  $a, b, c$ , which weakly depends on the temperature, as  $a = b = c = 1$  for simplicity.

For the nonthermal electron population with a power-law distribution, the emissivity  $j_{\nu,\text{pl}}$  is given by (Rybicki & Lightman 1979)

$$j_{\nu,\text{pl}} = C_{\text{pl}}^j \eta \frac{e^2 N_{\text{th}}}{c} a(\theta_e) \theta_e \nu_b \left( \frac{\nu}{\nu_b} \right)^{(1-p)/2}, \quad (17)$$

where

$$C_{\text{pl}}^j = \frac{\sqrt{\pi} 3^{p/2} (p-1)(p-2)}{4 (p+1)} \times \frac{\Gamma(p/4 + 19/12) \Gamma(p/4 - 1/12) \Gamma(p/4 + 5/4)}{\Gamma(p/4 + 7/4)}, \quad (18)$$

where  $\Gamma$  is the Gamma function.

In contrast to the previous studies (e.g., Özel et al. 2000), we here examine the spectral modification by the relativistic effect. The observed frequency  $\nu_{\text{obs}}$  in the inertial frame is related to the emitted frequency  $\nu$  in the comoving frame by

$$\nu_{\text{obs}} = \frac{\nu}{1+z}, \quad (19)$$

where  $z$  is the redshift originated from the bulk motion of the optically thin black-hole wind and the gravitational redshift, although we ignore the light-bending in this paper (cf. Hutsemékers & Surdej 1990; Dorodnitsyn 2009 for P Cyg profile of relativistic winds). Furthermore, the observed emissivities are also given as

$$j_{\nu,\text{th,obs}} = \frac{j_{\nu,\text{th}}}{(1+z)^3}, \quad (20)$$

$$j_{\nu,\text{pl,obs}} = \frac{j_{\nu,\text{pl}}}{(1+z)^3}. \quad (21)$$

Finally, under the optically-thin assumption, the comoving and observed luminosities become, respectively,

$$L = \int (j_{\nu,\text{th}} + j_{\nu,\text{pl}}) 2\pi r dr dz, \quad (22)$$

$$L_{\text{obs}} = \int (j_{\nu,\text{th,obs}} + j_{\nu,\text{pl,obs}}) 2\pi r dr dz. \quad (23)$$

In optically thin accretion flows thermal synchrotron and its Comptonization play an important role to the shape of the broad band spectrum (e.g., Kusunose & Takahara 1989; Narayan & Yi 1994; Mahadevan 1997; see also Park & Ostriker 2006). In particular, the Comptonized radiation is emitted in high energy spectrum. However, the purpose of this study is not to fit the spectrum, but to demonstrate the relativistic effect in the outflow. Hence, we ignore the Comptonization.

### 3. Results

Using a wind model and approximated synchrotron emissivities, we calculate spectra from hot, optically thin black-hole winds for various parameters.

The parameters of a wind model are the black hole mass  $M$ , the mass-outflow rate  $\dot{M}$ , the wind (terminal) velocity  $\beta$ , and the central temperature  $T_c$ , while the parameters of emissivity are the fraction  $\eta$ , the power-law index  $p$ , and the magnetic strength  $B$ . Of these, we fix  $M = 10^9 M_\odot$  and  $T_c = 10^{12}$  K, bearing in mind blazars and low luminosity active galaxies. The fraction of the nonthermal electron population is fixed as  $\eta = 0.04$ , using the recent results by Inoue et al. (2008). Hence, the rest parameters are  $\beta$ ,  $p$ ,  $B$ , and  $\dot{m}$ , where

$$\dot{m} \equiv \frac{\dot{M} c^2}{L_E} \quad (24)$$

is the mass-outflow rate normalized by the critical rate,  $L_E$  being the Eddington luminosity of the central object.

For wind velocity laws, we in turn examine two cases; constant and increasing cases.

#### 3.1. Constant Velocity

We first consider the relativistic effect of the wind bulk motion on the observed spectrum, which is of most interest in this study. Spectra for typical parameters are shown in figure 1.

In figure 1 the comoving and observed spectra are shown by thin dashed and thick solid curves, respectively, for several values of the wind velocity. The constant velocities are  $\beta = 0.1, 0.5, 0.9$  from top to bottom. Other parameters are fixed as  $\dot{m} = 10^{-3}$ ,  $p = 2.5$ , and  $B = 1$  gauss. Here, the magnetic field strength  $B$  is assumed to be constant spatially.

From figure 1, we first notice that the spectral intensity decreases as the wind velocity increases. This is because that the density of the observed region decreases as the wind velocity increases for the same  $\dot{m}$ .

Next, as the wind velocity increases, the observed spectral intensities become much more lower than the comoving ones, although the peak frequencies of the observed spectra shift toward the high frequency direction than those of the comoving ones. At first thought, the relativistic effect generally shifts the spectra toward a high energy

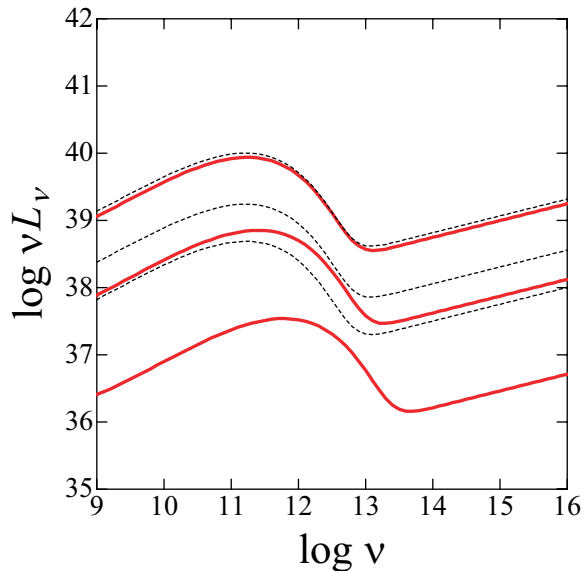


**Fig. 1.** Comoving spectra (thin dashed curves) and observed ones (thick solid ones) for  $\beta = 0.1, 0.5, 0.9$  from top to bottom. Other parameters are fixed as  $\dot{m} = 10^{-3}$ ,  $p = 2.5$ , and  $B = 1$  gauss.

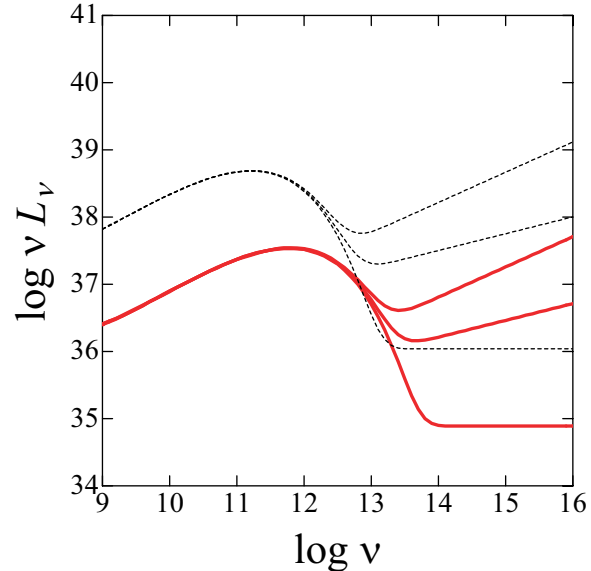


**Fig. 2.** Comoving spectra (thin dashed curves) and observed ones (thick solid ones) for  $p = 2.1, 2.5, 3$  from top to bottom. Other parameters are fixed as  $\beta = 0.9$ ,  $\dot{m} = 10^{-3}$ , and  $B = 1$  gauss.

regime. Indeed, in the optically thick case (Sumitomo et al. 2008), the observed spectra shift toward high frequency and high intensity directions, as the wind velocity increases. In the present case, the peak frequencies shift toward the high frequency direction, as expected. The spectral intensity, however, shift toward a low energy direction.

This is understood as follows. In the present optically thin wind, we can observe the receding part of the flow and the part moving the perpendicular directions as well as the approaching part. When the flow velocity is sufficiently relativistic, the emitted intensities from the approaching part become blueshift, but those from the receding and perpendicular parts become redshift. As a result, the total observed spectra become lower than the emitted ones.

Compared to the results by Özel et al. (2000), the shape of the peak spectrum in figure 1 is somewhat flat. This is because we assume the uniform magnetic field. If we assume the equipartition, i.e., the gas pressure equals to the magnetic pressure, the magnetic field strength  $B$  is proportional to  $r^{-5/2}$ . Thus, the shape of the peak spectrum will be more sharpened.

We further examine other parameter dependence of the present optically thin black-hole winds.

In figure 2 the comoving and observed spectra are shown by thin dashed and thick solid curves, respectively, for several values of the index  $p$ . The values of  $p$  are  $p = 2.1, 2.5, 3$  from top to bottom. Other parameters are fixed as  $\beta = 0.9$ ,  $\dot{m} = 10^{-3}$ , and  $B = 1$  gauss.

The steepness of the power-law part of the synchrotron emission is generally expected as  $L_\nu \propto \nu^{-(p-1)/2}$  (Rybicki & Lightman 1979). Since the Doppler effect does not change the power law steepness, the observed spectra shift

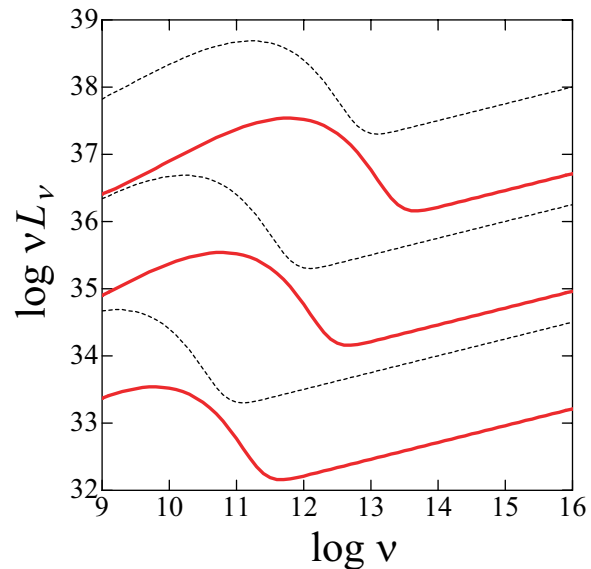


**Fig. 3.** Comoving spectra (thin dashed curves) and observed ones (thick solid ones) for  $B = 1, 0.1, 0.01$  gauss from top to bottom. Other parameters are fixed as  $\beta = 0.9$ ,  $\dot{m} = 10^{-3}$ , and  $p = 2.5$ .

toward the high frequency and low intensity directions in a self-similar manner, as the flow speed increases.

In figure 3 the comoving and observed spectra are shown by thin dashed and thick solid curves, respectively, for several values of the magnetic strength  $B$ . The values of  $B$  are  $B = 1, 0.1, 0.01$  gauss from top to bottom. Other parameters are fixed as  $\beta = 0.9$ ,  $\dot{m} = 10^{-3}$ , and  $p = 2.5$ .

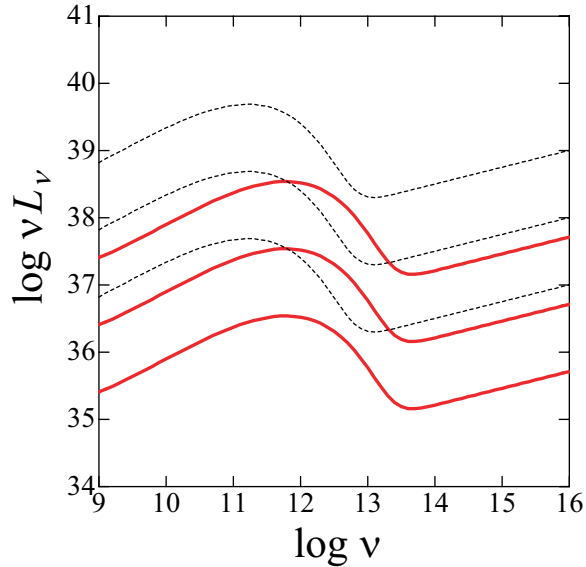


**Fig. 4.** Comoving spectra (thin dashed curves) and observed ones (thick solid ones) for  $\dot{m} = 10^{-2}, 10^{-3}, 10^{-4}$  from top to bottom. Other parameters are fixed as  $\beta = 0.9$ ,  $p = 2.5$ , and  $B = 1$  gauss.

As the magnetic field becomes weak, the peak frequency of thermal parts shifts toward the low frequency direction and the intensity becomes lower. On the other hand, the relativistic bulk motion shifts the peak frequency toward the high frequency direction.

In figure 4 the comoving and observed spectra are shown by thin dashed and thick solid curves, respectively, for several values of the mass-outflow rate  $\dot{m}$ . The values of  $\dot{m}$  are  $\dot{m} = 10^{-2}, 10^{-3}, 10^{-4}$  from top to bottom. Other parameters are fixed as  $\beta = 0.9$ ,  $p = 2.5$ , and  $B = 1$  gauss.

As is seen in figure 4, the mass-outflow rate does not affect the peak frequency, but only change the intensity. That is, as the mass-outflow rate decreases, the intensity simply decreases, since the gas density becomes low. As the flow velocity increases, the spectra shift toward high frequency and low intensity directions.

### 3.2. Increasing Velocity

In the realistic case, the hot gas must be accelerated from the very vicinity of the black hole to the outside, where the wind speed would reach the constant terminal one. In this subsection, we thus consider such a realistic wind velocity law, and compare the previous case of the constant velocity law.

As a velocity law, we adopt the monotonically increasing type, which is often used in the stellar wind:

$$\beta = \beta_0 + (\beta_\infty - \beta_0) \left(1 - \frac{R_0}{R}\right)^\alpha, \quad (25)$$

where the index  $\alpha$  is set to be unity for simplicity. The initial radius and velocity are also set to be  $R_0 = 2.0 r_g$  and  $\beta_0 = 0.1$ , respectively, while the terminal velocity  $\beta_\infty$  is left as a free parameter. Therefore, the parameters are

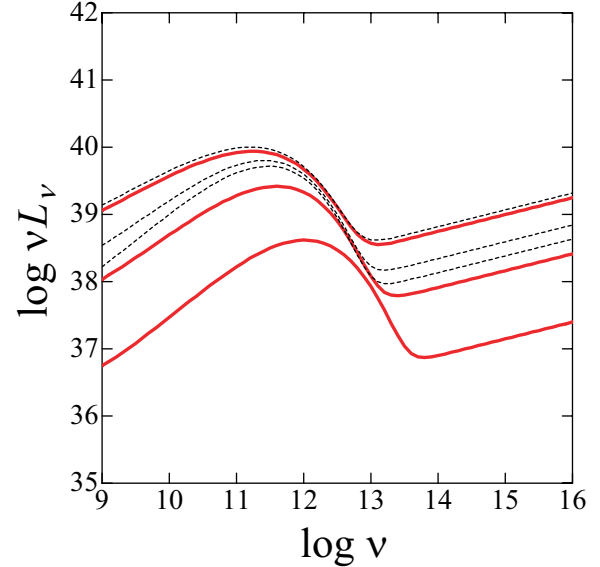


**Fig. 5.** Comoving spectra (thin dashed curves) and observed ones (thick solid ones) for  $\beta_\infty = 0.1, 0.5, 0.9$  from top to bottom. Other parameters are fixed as  $\dot{m} = 10^{-3}$ ,  $p = 2.5$ , and  $B = 1$  gauss.

$\beta_\infty$ ,  $p$ ,  $B$ , and  $\dot{m}$ .

In figure 5 the comoving and observed spectra are shown by thin dashed and thick solid curves, respectively, for several values of the terminal speed (see also figure 1). The values of the terminal speed are  $\beta_\infty = 0.1, 0.5, 0.9$  from top to bottom. Other parameters are fixed as  $\dot{m} = 10^{-3}$ ,  $p = 2.5$ , and  $B = 1$  gauss.

In the case of  $\beta_\infty = 0.1$  the wind profile is constant and the spectra is the same as the case of  $\beta = 0.1$  in figure 1. On the other hand, in the cases of  $\beta_\infty = 0.5$  (and 0.9), the wind is accelerating from the low speed to high speed, and the results are different from those shown in figure 1. For example, the comoving spectra do not change so much, compared with the constant velocity case. That is, the relativistic effect is somewhat suppressed. This is because in the accelerating wind the velocity of the central part, where the synchrotron emissivity is large, is small.

Moreover, the profiles of the thermal emission is different from those in the constant velocity case. This is because the thermal emission strongly depends on the density  $N_{\text{th}}$ , which also strongly depends on the velocity profile.

In figure 6 the comoving and observed spectra are shown by thin dashed and thick solid curves, respectively, for several values of the index  $p$  (see also figure 2). The values of  $p$  are  $p = 2.1, 2.5, 3$  from top to bottom. Other parameters are fixed as  $\beta_\infty = 0.9$ ,  $\dot{m} = 10^{-3}$ , and  $B = 1$  gauss.

As already stated, we notice that the spectral profile of the thermal part is rather different from the constant velocity case. Much more important is the total luminosity. Generally, in the realistic case with the increasing velocity law, the luminosity decreases as the terminal speed increases since the density decreases. However, we found

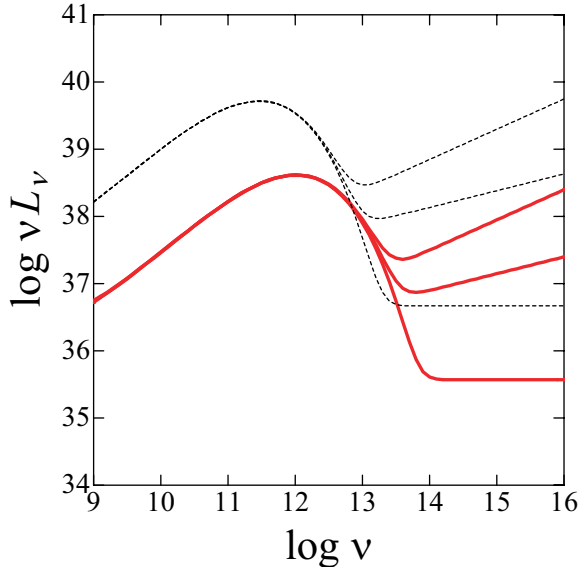


**Fig. 6.** Comoving spectra (thin dashed curves) and observed ones (thick solid ones) for  $p = 2.1, 2.5, 3$  from top to bottom. Other parameters are fixed as  $\beta_\infty = 0.9$ ,  $\dot{m} = 10^{-3}$ , and  $B = 1$  gauss.

that the luminosity is rather higher than that of the constant velocity case. This is also because in the increasing velocity case the This is because in the accelerating wind the velocity of the central part is small.

#### 4. Concluding Remarks

In this paper, we examined the observational appearance of hot, optically thin, relativistic, spherically symmetric black-hole winds from the observational point of view. We have calculated emitted and observed spectra of hybrid thermal-nonthermal synchrotron emissions, taking into account the relativistic effect in the high velocity regime. The spectral intensity generally decreases, as the wind velocity increases or the mass-outflow rate decreases.

We could see deeper inside the wind, as the velocity increases. This is the *relativistic* limb-darkening effect. This nature does not depend on the observer's direction. In addition, the luminosity in the observer's frame is remarkably enhanced by relativistic beaming effects along the observer's direction. These two effects mainly work as the luminosity enhancement of the relativistic outflow. We suggest that if the observed luminosity is used for the evaluation of the black hole mass, then the derived black hole mass will be overestimated.

We found that the intensity of the observed spectra decreases compared with that of the emitted ones, although the peak frequency shifts towards the high frequency direction. For example, in the cases of  $\beta = 0.9$  or  $\beta_\infty = 0.9$  the observed intensity becomes smaller than the emitted one more than about one order. This is because in the optically thin outflows we can see the far side flows that go away from the observer.

Furthermore, we found that the intensity of the constant velocity case becomes smaller than that of the accelerating case. This is because in the accelerated velocity case the central part has a low velocity. We thus carefully consider optically thin relativistic flows around a black hole such as Sgr A\*.

In the present study we did not solve the radiative transfer equation, while Özel et al. (2000) solved the radiative transfer to obtain the hybrid synchrotron spectra. We focus our attention on the relativistic effect of hot, optically thin black-hole winds, and the relativistic effect is generally important in the high frequency regime. In order to solve the spectra in the low frequency regime correctly, we should solve the radiative transfer equation as Özel et al. (2000) have done.

Moreover, we ignored the general relativistic bending of light, which becomes important at the very center of winds (Hutsemékers & Surdej 1990; Dorodnitsyn 2009 for P Cyg profile of relativistic winds). In the realistic situation winds would be accelerated at the very center. We should include these detailed behavior at the very center of winds in future.

Finally, we ignored the Comptonization in this paper (e.g., Kusunose & Takahara 1989; Narayan & Yi 1994; Mahadevan 1997; Park & Ostriker 2006). In the hot plasma, however, the emitted bremsstrahlung and synchrotron photons are generally upscattered by inverse Compton scattering. For example, the Compton-heated outflow was examined in details in Park and Ostriker (2006). Such a Comptonization works for the gas as cooling, and modifies the spectra (Rybicki and Lightman 1979). Although in order to demonstrate the relativistic effect we ignored the Comptonization in this paper, we should include the Comptonization to give more realistic spectra from the hot black-hole wind.

#### References

- Abramowicz, M. A., Novikov, I. D., & Paczyński B. 1991, ApJ, 369, 175
- Begelman, M. C. & Chiueh, T. 1988, ApJ, 332, 872
- Bisnovatyi-Kogan, G. S., & Lovelace, R. V. E. 1997, ApJ, 486, L43
- Colpi, M., Maraschi, L., & Treves, A. 1984, ApJ, 280, 319
- Dorodnitsyn, A.V. 2009, MNRAS, 393, 1433
- Fukue, J., & Sumitomo, N. 2009, PASJ, 61, in press
- Gammie, C.F., & Popham, R. 1998, ApJ, 498, 313
- Ghisellini, G., Haardt, F., & Fabian, A. C. 1993, MNRAS, 263, L9
- Ghisellini, G., Haardt, F., & Svensson, R. 1998, MNRAS, 297, 348
- Gruzinov, A., & Quataert, E. 1999, ApJ, 520, 849
- Hutsemékers, D., & Surdej, J. 1990, ApJ, 361, 367
- Inoue, Y., Totani, T., & Ueda, Y., 2008, ApJ, 672, L5
- Kato, S., Fukue, J., & Mineshige, S. 2008, Black-Hole Accretion Disks (Kyoto: Kyoto University Press)
- Kusunose, M., & Takahara, F. 1989, PASJ, 41, 263
- Li, H., Kusunose, M., & Liang, E. P. 1996, ApJ, 460, L29
- Mahadevan, R., Narayan, R., & Yi, I. 1996, ApJ, 465, 327
- Mahadevan, R. 1997, ApJ, 477, 585
- Medvedev, M. 2000, ApJ, 541, 811

- Narayan, R., & Yi, I. 1995, ApJ, 452, 710  
Narayan, R., McClintock, J.E., Yi, I. 1996, ApJ, 457, 821  
Özel, F., Psaltis, D. & Narayan, R., 2000, ApJ, 541, 234  
Park, M-G., & Ostriker, J.P. 2007, ApJ, 655, 88  
Quataert, E., & Gruzinov, A. 1999, ApJ, 520, 248  
Quataert, E., & Narayan, R. 1999, ApJ, 520, 298  
Rybicki, G.B., & Lightman, A.P. 1979, Radiative Processes in  
Astrophysics (New York: John Wiley & Sons)  
Sumitomo, N., Nishiyama, S., Akizuki, C., Watarai, K., &  
Fukue, J. 2008, PASJ, 59, 1043  
Zdziarski, A. A., Lightman, A. P., & Maciolek-Niedzwiecki, A.  
1993, ApJ, 414, L93